International Journal of Hydrogen Energy

CFD Analysis of Wall Function Effects on Flow Dynamics and Mixture Distribution in a Hydrogen Direct Injection Engine

--Manuscript Draft--

Manuscript Number:	
Article Type:	Full Length Article
Section/Category:	Heat Engines / Combustion / Heat Transfer
Keywords:	Hydrogen, Direct Injection, Computational Fluid Dynamics, Wall functions, Mixture Distribution
Corresponding Author:	Srinivasa Krishna Addepalli, Ph.D. Indian Institute of Technology Tirupati Lemont, Illinois UNITED STATES
First Author:	Srinivasa Krishna Addepalli, Ph.D.
Order of Authors:	Srinivasa Krishna Addepalli, Ph.D.
	Arunkumar Venkatesan, Bachelor of Technology
	Sneha M Srinivas, Bachelor of Technology
Abstract:	Direct injection (DI) of gaseous hydrogen into the combustion chamber of internal combustion (IC) engines is considered a promising method to circumvent the issues of pre-ignition and backfire. However, a significant research focus is required to implement this technology in modern IC engines successfully. The present study focuses on a numerical investigation of mixture preparation in a spark-ignition IC engine where gaseous hydrogen is directly injected into the combustion chamber at a pressure of 100 bar. Numerical simulations on the engine were carried out at an engine speed of 1500 rev/min at a high tumble. The flow turbulence was modeled using the renormalized group (RNG) k-ε model. Different wall functions were used to model the flow and turbulence characteristics near the walls of the combustion chamber. The mixture distribution in the combustion chamber obtained by employing different wall functions was compared with the optical data acquired from planar laser-induced fluorescence (PLIF) measurements. The results showed that the Enhanced wall function and the Analytical wall function resulted in good agreement between the numerical analysis and optical measurement data compared to the other models.

To:

The Editor
International Journal of Hydrogen Energy

Dear Sir,

I am herewith submitting our paper titled "**CFD Analysis of Wall Function Effects on Flow Dynamics and Mixture Distribution in a Hydrogen Direct Injection Engine**" authored by Srinivasa Krishna Addepalli, Arunkumar V, and Sneha M S, for consideration for publication in your esteemed journal. The address of the corresponding author is as follows. This is an original paper that has neither previously, nor simultaneously, in whole or in part been submitted anywhere else.

Dr. Srinivasa Krishna Addepalli
Ramanujan Fellow,
Department of Mechanical Engineering,
Indian Institute of Technology Tirupati,
Off Yerpedu-Venkatagiri Road,
Tirupati, Andhra Pradesh, 517619,
India

Thanking you,

With Regards,

Yours sincerely

Srinivasa Krishna Addepalli

Suggested Reviewers:

1. **Dr. Michele Battistoni**
   Associate Professor
   ENGINEERING DEPARTMENT
   ING-IND / 08 - FLUID MACHINES
   E-mail: michele.battistoni@unipg.it
   Phone: +39 0755853749

2. **Dr. Rafig Babayev**
   Simulation Engineer
   Volvo Group Trucks Technology
   Email: rafik.babayev95@gmail.com; rafig.babayev@kaust.edu.sa; rafig.babayev@chalmers.se

3. **Dr. Ranga Dinesh Kahanda Koralage**
   Lecturer in Energy Technologies
   University of Southampton
   Email: Dinesh.Kahanda-Koralage@soton.ac.uk
   Phone: (023) 8059 2872

Highlights:

The impact of different wall functions on the mixture distribution is compared

The Enhanced and Analytical wall functions perform better than the Standard, Scalable, and Non-equilibrium wall functions

The Enhanced and Analytical wall functions result in higher velocity and higher mole fractions near the wall

CFD Analysis of Wall Function Effects on Flow Dynamics and Mixture Distribution in a Hydrogen Direct Injection Engine

Srinivasa Krishna Addepalli, Arunkumar V*, and Sneha M S*

Department of Mechanical Engineering

Indian Institute of Technology Tirupati – 517619

Andhra Pradesh, India

***Equal Contributors**

Abstract: Direct injection (DI) of gaseous hydrogen into the combustion chamber of internal combustion (IC) engines is considered a promising method to circumvent the issues of pre-ignition and backfire. However, a significant research focus is required to implement this technology in modern IC engines successfully. The present study focuses on a numerical investigation of mixture preparation in a spark-ignition IC engine where gaseous hydrogen is directly injected into the combustion chamber at a pressure of 100 bar. Numerical simulations on the engine were carried out at an engine speed of 1500 rev/min at a high tumble. The flow turbulence was modeled using the renormalized group (RNG) k-ε model. Different wall functions were used to model the flow and turbulence characteristics near the walls of the combustion chamber. The mixture distribution in the combustion chamber obtained by employing different wall functions was compared with the optical data acquired from planar laser-induced fluorescence (PLIF) measurements. The results showed that the Enhanced wall function and the Analytical wall function resulted in good agreement between the numerical analysis and optical measurement data compared to the other models.

Keywords: *Hydrogen, Direct Injection, Computational Fluid Dynamics, Wall functions, Mixture Distribution*

Nomenclature:

AMR	Adaptive Mesh Refinement
CAD	Crank Angle Degree
CFD	Computational Fluid Dynamics
CI	Compression-Ignition
DI	Direct Injection
ECN	Engine Combustion Network
IC	Internal Combustion
IVC	Intake Valve Closing
LES	Large Eddy Simulation
PFI	Port Fuel Injection

PIV	Particle Image Velocimetry
PLIF	Planar Laser-Induced Fluorescence
RANS	Reynolds Averaged Navier Stokes
RNG k- ε	Renormalization group k- ε
ROI	Rate of Injection
SI	Spark Ignition
SOI	Start of Injection
TDC	Top Dead Center

1. Introduction

In today's energy landscape, hydrogen stands out as a versatile energy carrier with potential applications across various sectors [1]. Hydrogen finds applications in storing the intermittent energy generated by renewable energy sources [2-6]. It is also used to feed fuel cells [7-11]. Further, hydrogen finds application as a fuel for internal combustion (IC) engines due to its potential for zero carbon emissions and high energy efficiency [12-17]. Using hydrogen as a fuel for IC engines is particularly appealing because it can take advantage of the well-established combustion and emission control technologies already developed for these engines. With the latest advances in direct fuel injection technology and electronic fuel management, it is now possible to inject gaseous hydrogen directly into the combustion chamber [18], effectively eliminating the issues of backfire and pre-ignition commonly found in conventional port fuel-injected engines [19-21].

Injecting gaseous hydrogen directly into the combustion chamber allows it to mix with the trapped fresh charge. Proper mixture formation is essential for achieving the desired performance and emission characteristics in a direct injection hydrogen-fueled IC engine. Early injection timing produces a homogeneous mixture, while late injection results in a stratified mixture. Recent research has underscored the significance of mixture distribution in hydrogen-fueled engines. Studies by Huang et al. [22] and Zhen Hu et al. [23] have highlighted the critical role of mixture formation in determining combustion performance and efficiency in direct injection hydrogen engines. Scalambro et al. [24] found that optimizing combustion chamber geometry improves mixture homogeneity, while Luo et al. [25] demonstrated that delayed injection worsens mixture uniformity, leading to higher NOx emissions. Wu et al. [26] emphasized the importance of discretization schemes for accurate mixing simulation, and Wang et al. [27] showed how injection timing influences mixture stratification and overall engine efficiency. Additionally, Salazar et al. [28] and Scarcelli et al. [29] pointed to the importance of injector design and pre-injection flow dynamics in achieving effective in-cylinder mixing. Sukumaran et al. [30] suggested early injection and strategic injector placement to enhance uniformity, and Xiumin et al. [31] demonstrated hydrogen's potential to reduce emissions compared to gasoline. Fu et al. [32] highlighted the sensitivity of ultra-lean combustion to mixture distribution. These studies collectively underscore the necessity of precise simulation and control of mixture distribution to optimize hydrogen engine performance and emissions.

Computational Fluid Dynamics (CFD) is crucial in the design and development of modern internal combustion engines. With increasing computational power and precise mathematical models, CFD enables detailed analysis of fluid flow, combustion, and emission characteristics in engines, thereby reducing experimental costs in the engine design process. Early injection of hydrogen gas into the combustion chamber at high pressure results in a possible interaction between the turbulent gas jet and the combustion chamber walls. Accurately modeling the interaction between the fuel-air mixture and the walls of the combustion chamber is essential, as it directly influences velocity and shear stress in the boundary layer. These factors impact the mixture distribution within the chamber, affecting overall combustion and engine performance. Effective modeling must address the complexities of wall-bounded turbulent flows, characterized by pronounced viscosity effects and large gradients in solution variables near the wall.

Traditionally, simulating turbulent flows involves dividing the flow domain into distinct layers: the viscous sublayer, the buffer layer, and the log-law (or inertial) region as shown in Fig. 1. The viscous sublayer, corresponding to a dimensionless wall distance y+ of less than 5, is dominated by viscous effects and steep velocity gradients. The flow in this region follows the "linear velocity law," where the dimensionless velocity u+ is proportional to y+. As we move away from the wall, the flow enters the logarithmic region (log-law region), where y+ is greater than 30. Here, turbulence effects dominate viscous effects, and the velocity profile follows a logarithmic distribution. Between these regions lies the buffer layer ($5 < y+ < 30$), a transition zone where both viscous and turbulent effects are significant. This layer's velocity profile is not well-defined, making accurate modeling challenging.

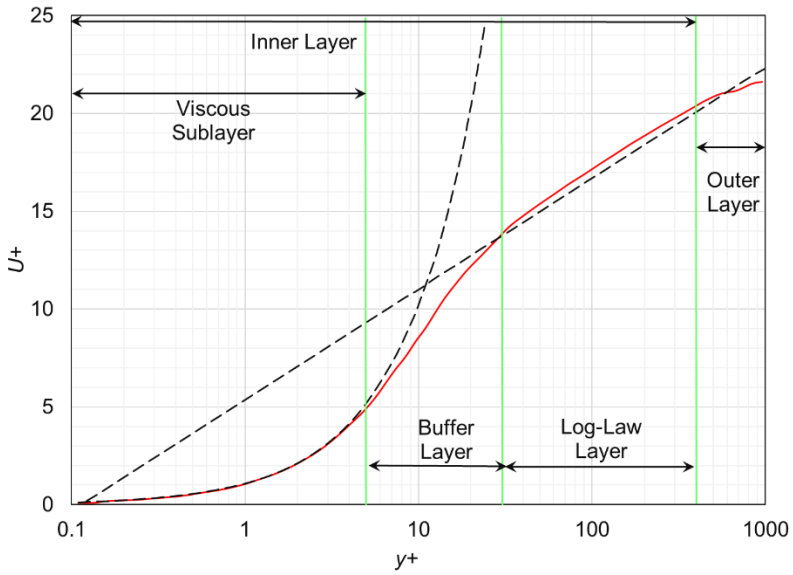

Fig. 1. Schematic description of different regimes in the turbulent boundary layer

Popular turbulence models, such as the k−ε model, are valid only in fully developed turbulence regions and perform poorly close to the wall. Two common approaches to address this issue are

(i) Integrating the turbulence model to the wall, requiring a fine computational grid to capture the viscous sublayer accurately, with the first cell ideally placed at a y+ value of 1. This approach is suitable for flows the low Reynolds numbers and it provides detailed results but demands substantial computational resources [33]. (ii) Modelling the near-wall parameters using wall functions which are empirical equations that bridge the gap between the wall and the region of fully developed turbulence, allowing for a coarser grid and reducing computational costs [34, 35]. In this study, we adopt the latter approach to assess near-wall parameters and the resulting mixture distribution when a high-pressure hydrogen jet interacts with the walls of the combustion chamber in a direct injection spark ignition engine. The engine geometry was adopted from Sandia's optical hydrogen engine [36] equipped with a centrally mounted single-hole injector to inject gaseous hydrogen. During the compression stroke, the injected hydrogen gas interacts with the walls of the combustion chamber. Accurately modeling the complex interactions between the hydrogen-air mixture and the walls of the combustion chamber, without relying on an excessively fine computational mesh near the wall, is essential. These interactions directly affect boundary layer dynamics and, consequently, the mixture distribution within the combustion chamber. Simulations are carried out using some popular wall functions and the results are compared with the experimental data obtained from Planar Laser-Induced Fluorescence (PLIF) measurements [36, 37], which are publicly available on Sandia's website [38]. Several numerical studies have been conducted on the engine considered in this research, primarily focusing on simulating the mixture distribution process [39-45]. However, the present study uniquely highlights the impact of different wall functions on mixture distribution within the combustion chamber, offering insights that enhance understanding and improve the accuracy of simulations using Reynolds Averaged Navier Stokes (RANS) based turbulence models.

2. Experimental Setup

Experimental studies were conducted by Salazar and Kaiser [36] on a single-cylinder SI engine using Particle Image Velocimetry (PIV) and PLIF techniques. This engine, installed at Sandia National Laboratory, is equipped to inject gaseous hydrogen directly into the combustion chamber through a centrally located Westport Direct Injection (DI) injector. The engine specifications are mentioned in Table. 1. The engine features dual intake and exhaust ports, a pentroof head, and a flat piston. The flow field and mixture distribution were studied at a "high tumble" (with a tumble plate in the intake port) and a "low tumble" (without a tumble plate in the intake port) configurations.

The experiments were carried out under non-firing conditions. The engine speed was maintained at 1500 rpm while Nitrogen gas was supplied to the intake manifold. The single-hole injector had a diameter of 1.46 mm, and it is oriented at 50^0 angle with the cylinder axis. Hydrogen gas was injected into the combustion chamber at 100 bar pressure. The nominal start of injection was maintained at -140 CAD. Considering the injector's hydraulic delay, the actual injection event began at -137 CAD and concluded at -119.5 CAD. Acetone was used as a tracer to seed the

hydrogen for PLIF measurements [36]. The experiments captured the hydrogen concentration (mole fraction) and the velocity field on the central vertical plane.

Table. 1 Engine Specifications [38]

Bore	92 mm
Stroke	85 mm
Displacement Volume	565 cm^3
Compression Ratio	10.91
Intake Valve Opening (IVO)	-373^0 CA
Intake Valve Closing (IVC)	-140^0 CA
Exhaust Valve Opening (EVO)	131^0 CA
Exhaust Valve Closing (EVC)	-355^0 CA
Injection pressure	100 bar

3. CFD Methodology

3.1. Engine Geometry and Mesh Generation

Fig. 2 (a) shows the computational domain used in this study. Fig. 2 (b) shows the cut section of the cylinder head in the front view along with the orientation of the injector. Fig. 2 (c) shows the central vertical plane passing through the injector on which the PIV and PLIF images were taken. CFD simulations were carried out using the commercial CFD software CONVERGE (Version 3.1.8). A structured mesh using the cut-cell Cartesian approach was generated in the computational domain during the run time. Mesh refinement in the computational domain was performed using adaptive mesh refinement (AMR) based on velocity and temperature gradients. AMR refines the cells if the absolute value of a parameter is above a user-specified value. Further mesh refinement was carried out using fixed embedding at some of the strategic locations, the valve seats, and the walls where the gradients are higher. Based on the previous study [42], four mesh layers with a cell height of 0.25 mm were created on the piston, liner, and cylinder head boundaries. An inlaid mesh with a cell size of 0.125 mm, as described by Addepalli et al., [42] was created near the injector's exit to resolve the nozzle's near field accurately. The cross-section of the mesh generated in this study at -130 CAD is shown in Fig. 3. As a matter of convention, 0 CAD was considered to represent combustion top dead center (TDC). Thus, a full cycle runs from -360 CAD to 360 CAD. All the simulations were carried out from the intake valve opening (IVO) to combustion TDC.

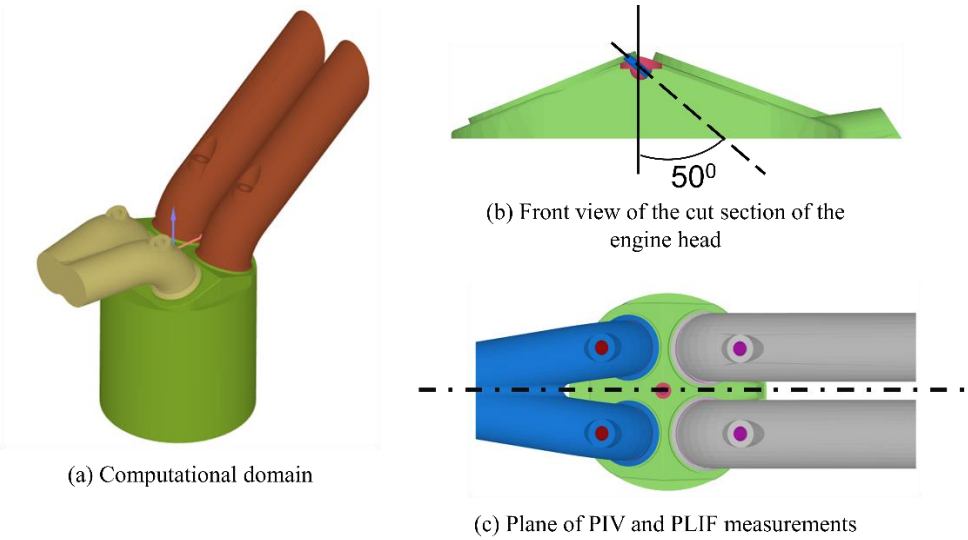

(a) Computational domain

(b) Front view of the cut section of the engine head

(c) Plane of PIV and PLIF measurements

Fig. 2. Details of engine geometry

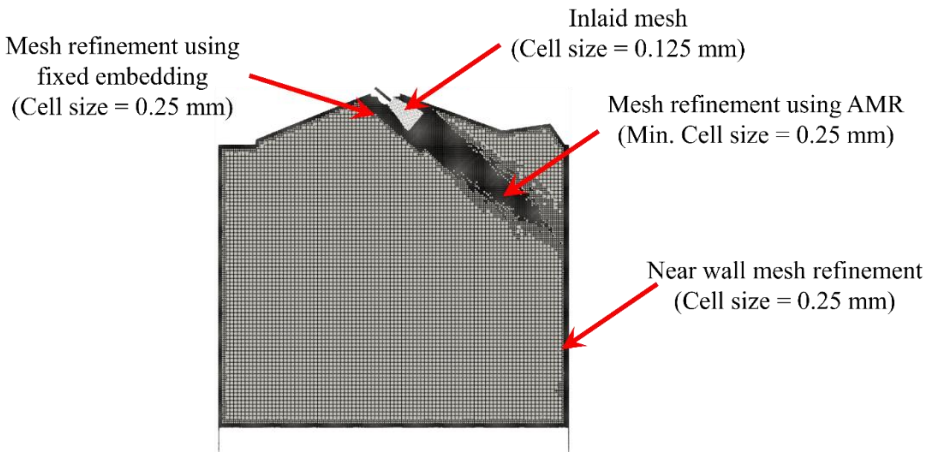

Fig. 3. Cross section of computational mesh at -130 CAD

3.2. Boundary Conditions

The computational domain was initialized with Nitrogen gas to replicate the experimental conditions. Based on the information on Sandia website [38], crank angle resolved cylinder pressure data as shown in Fig. 4 were imposed on the inlet and outlet of the computational domain. The inlet was maintained at 309.15 K and the walls of the computational domain were maintained at 353 K. Fig. 5 shows the valve lift profile used to specify the valve motion as given on the Sandia website. Based on the earlier study [42], [45] the injector was assumed as a duct of length 5.5 mm and diameter of 1.46 mm. The cross-section of the single-hole injector used in the study is shown in Fig. 6. Fig. 7 shows the Rate of Injection (ROI) profile for the injector as specified on the Sandia website. [38]. The specified ROI profile is in the shape of a trapezoid with a ramp up/down of 1 CAD.

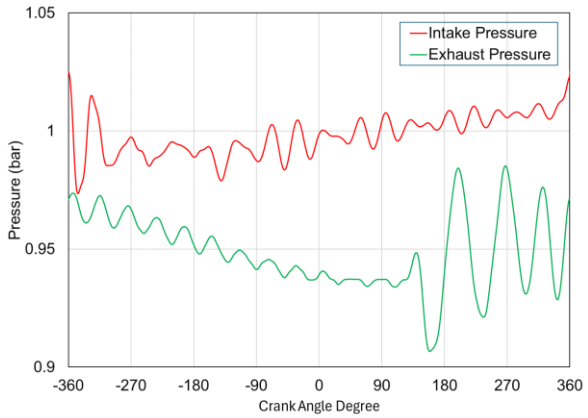

Fig. 4. Inlet and outlet pressure boundary conditions

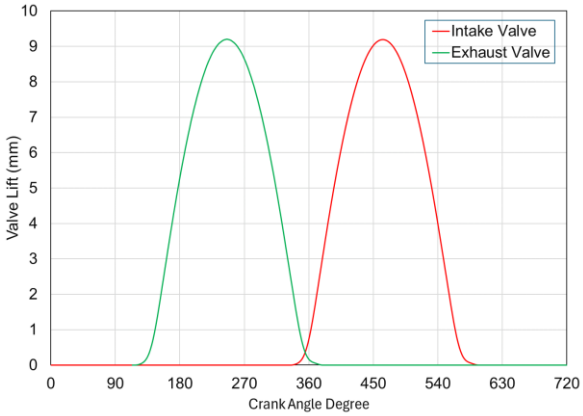

Fig. 5. Valve lift profiles

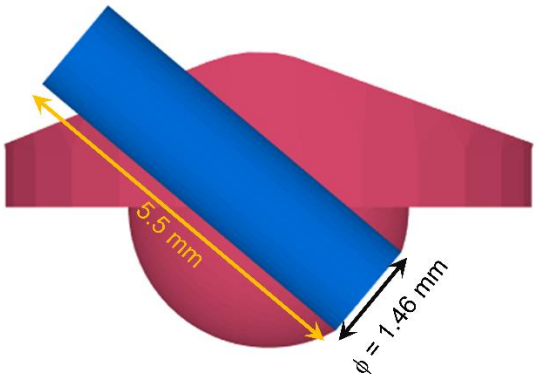

Fig. 6. Cross section of the injector geometry

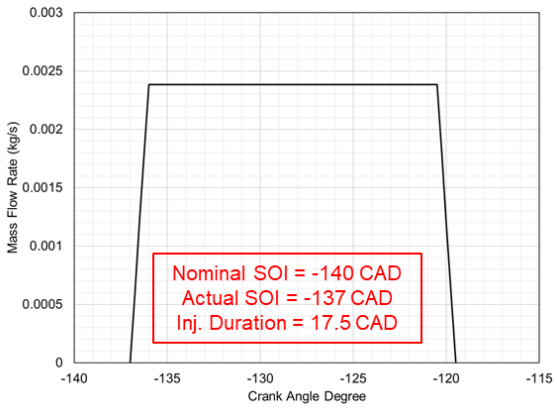

Fig. 7. Rate of injection profile [42] [45]

4. CFD Models

The fluid flow was solved using the Navier-Stokes equations for mass, momentum, and energy. Redlich Kwong equation of state was chosen in this study, to accurately predict the Joule-Thompson inversion curve for hydrogen [46]. Reynolds averaged Navier Stokes (RANS) based Renormalized group (RNG) k-ε model was used to model flow turbulence.

4.1. Wall Functions

In the present study, the effect of different wall functions on the behavior of the mixture preparation is analyzed in a hydrogen-fueled direct injection spark ignition engine. Hydrogen gas is directly injected into the engine cylinder in the compression stroke after the intake valves close (IVC), through a centrally mounted single-hole injector as explained earlier. The resulting hydrogen jet, while mixing with the surrounding air, first impacts the right liner wall, travels downwards along the liner, moves left along the flat piston surface, ascends the left liner wall, and finally returns to the injector location, all of which happens during the compression stroke. Thus, the hydrogen-air mixture interacts with the walls of the combustion chamber as the piston moves upwards through the compression stroke.

In the present study, the absolute height of the first cell from the walls of the combustion chamber is maintained at 0.25 mm, resulting in a y+ for the walls of the combustion chamber in the range of 20 and 100 during the simulations. By using standard calculation, it can be observed that the first cell falls in the inner log-law region of the boundary layer (either in the buffer layer or in the log-law layer). To capture the gradients near the wall by integrating the turbulence model onto the wall, it is required to maintain the cell size in that region in the order of a few microns or less, significantly increasing the total computational time.

Accurately modeling the interaction between the mixture and the combustion chamber walls is crucial because it directly affects the velocity and shear stress in the boundary layer, influencing the mixture distribution within the chamber. Therefore, in this study, five popularly used wall functions viz., Standard, Scalable, Non-equilibrium, Enhanced, and Analytical models are used to simulate the flow turbulence characteristics near the walls of the combustion chamber. The simulation results in terms of the mixture distribution in the combustion chamber are compared with the experimental PLIF images [38]. This section provides a brief mathematical description of the different wall functions used in this study.

4.1.1. Standard Wall Function

In this model, the first cell next to the wall is assumed to be within the log-law region. The following equation (Eq.1) calculates the specific dissipation rate (ε_p) at the cell centroid adjacent to the wall.

$$\varepsilon_p = \frac{C_\mu^{\frac{3}{4}} k_p^{\frac{3}{2}}}{\kappa y_p} \tag{1}$$

C_μ is the model constant

k_p is the turbulent kinetic energy

y_p is the distance from the wall to the cell centroid

κ is the von Karman's constant

4.1.2. Scalable Wall Function

The scalable wall function adjusts the log-law assumption of the standard wall function. It scales down the influence of the wall function when the adjacent cell is in the buffer region of the boundary layer, improving accuracy.

$$\varepsilon_p = \frac{C_\mu^{\frac{3}{4}} k_p^{\frac{3}{2}}}{\kappa\, y_p^*} \tag{2}$$

$$y_p^* = \max\left(y_p,\, y_p^{lim}\right) \tag{3}$$

Where y_p^{lim} = 11.05.

Using this formulation, if the first cell centroid falls within the log-law region of the boundary layer, the scalable wall function replicates the behavior of the standard wall function.

4.1.3. Non-Equilibrium Wall Function

The non-equilibrium wall function [47] enhances the mean velocity to account for pressure-gradient effects, utilizing a two-layer model to compute TKE in the cells adjacent to walls. The model assumes that the wall-neighboring cells have a velocity profile that is comprised of a viscous sublayer and a log-law turbulent layer, thereby addressing distortions caused by pressure gradients that invalidate local equilibrium assumptions regarding TKE production and destruction rates. However, mean temperature and species mass fraction are determined using the standard wall function within this framework.

The log-law for mean velocity sensitized to the pressure gradients is

$$\frac{\psi C_\mu^{\frac{1}{4}} k^{\frac{1}{2}}}{\tau_w/\rho} = \frac{1}{\kappa}\ln\left(E\,\frac{\rho C_\mu^{\frac{1}{4}} k^{\frac{1}{2}} y}{\mu}\right) \tag{4}$$

$$\psi = U - \frac{1}{2}\frac{dp}{dx}\left(\frac{y_v}{\rho\kappa\sqrt{k}}\ln\left[\frac{y}{y_v}\right] + \frac{y-y_v}{\rho\kappa\sqrt{k}} + \frac{y_v^2}{\mu}\right) \tag{5}$$

y_v is the physical viscous sublayer thickness

Ψ = Mean velocity

U = local velocity

The profile assumptions made are as follows:

	Shear Stress (τ_t)	Turbulent Kinetic Energy (k)	Turbulent Dissipation Rate (ε)
$y < y_v$	0	$\left(\frac{y}{y_v}\right)^2 k_p$	$\frac{2\nu k}{y^2}$
$y > y_v$	τ_w	k_p	$\frac{k^{\frac{3}{2}}}{C_l^* y}$

Where, $C_l^* = \kappa C_\mu^{-3/4}$

4.1.4. Enhanced Wall Function

The Enhanced wall function employs a two-layer method that integrates a modified law-of-the-wall for the logarithmic layer with an expression for the viscous sublayer. This wall function is insensitive to near-wall grid spacing, allowing the first cell from the wall to be positioned in the

viscous sublayer, the log-law region, or the buffer region between them without causing significant errors. Additionally, the Enhanced wall function considers the effects of pressure gradients, heat transfer, and compressibility in the momentum equation. The additional complexity of this model results in greater computational expense. However, this model performs better when near-wall pressure gradients and heat transfers are important.

The compressible log-layer law-of-the-wall [48] with heat transfer and pressure gradient is as follows:

$$\frac{du_l^+}{dy^+} = \frac{1}{\kappa y^+}(1+\alpha y^+)^{1/2}(1+\beta u_l^+ - \gamma[u_l^+]^2)^{1/2} \quad (6)$$

α is the pressure gradient parameter

β is the heat transfer parameter

γ Is the compressibility parameter

Within the viscous sublayer, pressure effects are neglected, and the velocity is given as

$$u_{vis}^+ = y^+ \quad (7)$$

The Enhanced wall function blends the solution of Eq. (6) and Eq. (7) based on a blending coefficient Γ

$$\Gamma_e = \frac{0.001(y^+)^4}{1+y^+} \quad (8)$$

The blended turbulent dissipation rate ε is calculated as follows,

$$\varepsilon = \exp(-\Gamma_e)\,\varepsilon_{vis} + \exp(-1/\Gamma_e)\,\varepsilon_l \quad (9)$$

where,

$\varepsilon_l = \frac{C_\mu^{\frac{3}{4}} k^{\frac{3}{2}}}{\kappa y}$ and $\varepsilon_{vis} = \frac{k^{\frac{3}{2}}}{\kappa y}$

4.1.5. Analytical Wall Function

The Analytical wall function utilizes analytic functions derived from integrating simplified momentum and energy equations near the wall. This approach is suitable for smooth walls. The model encompasses functions for near-wall shear stress, heat flux, turbulent viscosity, turbulent kinetic energy production, and turbulent dissipation.

The transition from the log-law region to the viscous sublayer occurs at $y_p^* = y_v^*$

$$y_p^* = y_p \frac{\rho\sqrt{k_p}}{\mu}$$

μ is molecular viscosity and $y_v^* = 10.7$

When $y_p^* > y_v^*$, cell p is in the log-law region

When $y_p^* < y_v^*$, cell p is in the viscous sublayer

The turbulent dissipation at cell p (ε_p) is given by,

$y_\varepsilon \geq y_p$	$\frac{2\mu k_p}{\rho y_\varepsilon^2}$
$y_\varepsilon \leq y_p$	$\frac{k_p^{3/2}}{c_l y_p}$

$y_\varepsilon = y_\varepsilon^* \frac{\mu}{\rho\sqrt{k_p}}$ and $y_\varepsilon^* = 5.1$ and $c_l = 2.55$

5. Results and Discussion

This section presents a comparison of the mixture distribution on the central vertical plane of the engine cylinder (refer to Fig. 2) from the simulations with the experimental results. The mixture distribution obtained using different wall functions is further analyzed by examining the gas velocity and hydrogen mole fraction profiles close to the right liner wall at discrete crank angles.

5.1. Impact of Wall Function Approaches on Mixture Distribution:

Fig. 8 shows the comparison of the mixture mole fraction on the central vertical plane of the engine cylinder at various crank angles from CFD using different wall functions against the experimental PLIF data. The range of crank angles presented in Fig. 8 corresponds to discrete events during the compression stroke. The mixture distribution in the pentroof region has been made translucent to provide a meaningful comparison between the experiments and simulations. Further, a dynamically varying scale has been used to represent the hydrogen mole fraction in the engine cylinder. As discussed by Addepalli et al. [42] the optical data suggests that the edge of the hydrogen jet is more dispersed probably due to the high diffusivity of hydrogen. It could also be due to phase averaging carried out during the postprocessing of the PLIF data [42].

The distribution of injected hydrogen within the combustion chamber can be attributed to three key factors: (i) the momentum created by high-pressure gas injection, which primarily drives jet evolution during the injection phase, (ii) the in-cylinder gas motion, which carries the hydrogen cloud due to hydrogen being lighter than nitrogen, and (iii) the highly diffusive nature of hydrogen. Additionally, the upward movement of the piston also contributes to the momentum of the gas inside the combustion chamber by imparting a bulk movement to it. At -130 and -120 CAD, while the injection event is still ongoing, the development of the hydrogen mixture cloud along the right liner wall and the piston surface is driven by the high momentum of the injected gas. Qualitatively, the mole fraction of the mixture from the CFD results appear to closely match the experimental results for all the different wall functions used at these crank angles. However, a further quantitative analysis is required to substantiate the qualitative observations, which is presented in the next section. Starting from -110 CAD, the evolution of mixture distribution in the combustion chamber is mainly due to the in-cylinder gas motion, the upward movement of the piston, and the diffusivity of the hydrogen. As the hydrogen cloud passes over the liner wall, different wall

functions result in different shear stresses and gas velocities near the walls resulting in variations in the mixture distribution.

At –110 CAD, the distance between the tip of the mixture cloud along the piston surface and the left liner wall for the Analytical and Enhanced wall functions closely matches the experimental results. However, for the Standard, Scalable, and Non-equilibrium wall functions, this distance is greater than that observed in the experiments. Additionally, the Analytical and Enhanced wall functions show a richer mixture in the top right corner of the plane, consistent with the experimental results while it is not observed in the other models. Further, the mixture cloud traveling along the piston surface for the Analytical and Enhanced wall functions appears more dispersed as observed in the experiments. The variations observed in the mixture distribution for different wall functions are further amplified as the piston moves upwards in the compression stroke.

At –100 CAD the mixture cloud approaches the left liner wall for the Analytical and Enhanced wall functions. In contrast, the other models show a larger gap between the mixture cloud and the left liner wall. Further, the Enhanced wall function shows a better dispersion inside the mixture cloud on the piston surface as is also evident from the experiments. The mixture in the top right corner is also noticeably richer for the Analytical and Enhanced wall functions compared to the other wall functions. At –85 CAD, the mixture travels a longer distance along the left liner wall for the Analytical and Enhanced wall functions than the Standard, Scalable, and Non-Equilibrium models, a trend that aligns with the experimental results. The Analytical and Enhanced wall functions continue to reproduce similar trends as in the experimental results at –70 CAD. The mixture approaches the injector location for the Analytical and Enhanced wall functions at –55 CAD, however, there is a larger gap between the leading edge of the mixture cloud and the injector for the Standard, Scalable, and Non–equilibrium wall functions. Although the injector location is not visually accessible in the experiments, the Analytical and Enhanced wall functions seem to replicate the mixture distribution in a way that closely matches the experimental results.

At –40 CAD and –30 CAD the experimental results suggest that the mixture tends to approach the injector after passing over the left liner wall and along the left half of the cylinder head. The CFD simulations qualitatively suggest that the mixture distribution for the Standard, Scalable, and Non-equilibrium wall functions is similar. They show a richer mixture cloud of almost similar size and spread in the left half of the combustion chamber, and a comparatively leaner mixture cloud of smaller size in the right half of the combustion chamber. A thin region separating the leaner mixture cloud on the right from the richer mixture cloud on the left in the combustion chamber contains almost no hydrogen (represented by a blue color). However, for the Analytical and Enhanced wall functions, the mixture appears more dispersed within the right and left halves of the combustion chamber compared to the other wall functions, showing a better match with the experiments. Additionally, the region between the right and left mixture clouds has a certain amount of hydrogen (represented by green color) as in the experimental observations. Further,

upon closer inspection, there is a slight difference in the mixture distribution between the Enhanced and Analytical wall functions at -30 CAD. However, due to the limited size of the observation window, it is difficult to definitively determine which one more closely aligns with the experimental results.

Overall, comparing the mixture mole fraction from CFD simulations with various wall functions to the experimental results indicates that the Enhanced and Analytical wall functions provide a closer match to the experimental data than the Standard, Scalable, and Non-equilibrium wall functions.

5.2. Impact of Wall Functions on the Near-Wall Velocity and Mole Fraction

The wall functions are used to model the velocity near the wall based on the distance of the centroid of the first cell (near the wall) from the wall. The other quantities are estimated based on the equations discussed in Section 4. The velocity of the gas, TKE, and the turbulent dispersion near the wall are some of the important parameters that influence the mixture distribution patterns in the combustion chamber. Further, in this study, the hydrogen jet hits the right liner wall of the combustion chamber during the initial phase of the injection event. Thus, the interaction of the mixture with the right liner wall is going to influence the mixture distribution in the combustion chamber at the subsequent crank angles during the compression stroke. Therefore, in this section, the variation of near wall velocity and mole fraction of hydrogen gas, along the right liner wall at discrete crank angles is plotted to further analyze the differences in the mixture distribution using different wall functions. Fig. 9 shows a blown-up schematic of the line along which the data is extracted and presented in this section.

Fig. 10 shows the variation of velocity along the right liner wall at -125 CAD, -110 CAD, and -100 CAD respectively for different wall functions. In Fig. 10, -125 CAD corresponds to an event when the hydrogen is still being injected into the combustion chamber, whereas the other two crank angles (-110 CAD and -100 CAD) correspond to the events after the end of fuel injection. The x-axis in Fig. 10 shows the distance along the left liner wall non-dimensionalized with the stroke length, which varies between 0 (near to spark plug location) to ~0.8 (near to the piston surface) at -125 CAD. For -110 CAD and -100 CAD, the maximum distance along the liner will be less than 0.8. The x and y axes for Fig. 10 (a), (b), and (c) have been set to different scales to better visualize the variations in flow property predictions across the different wall functions.

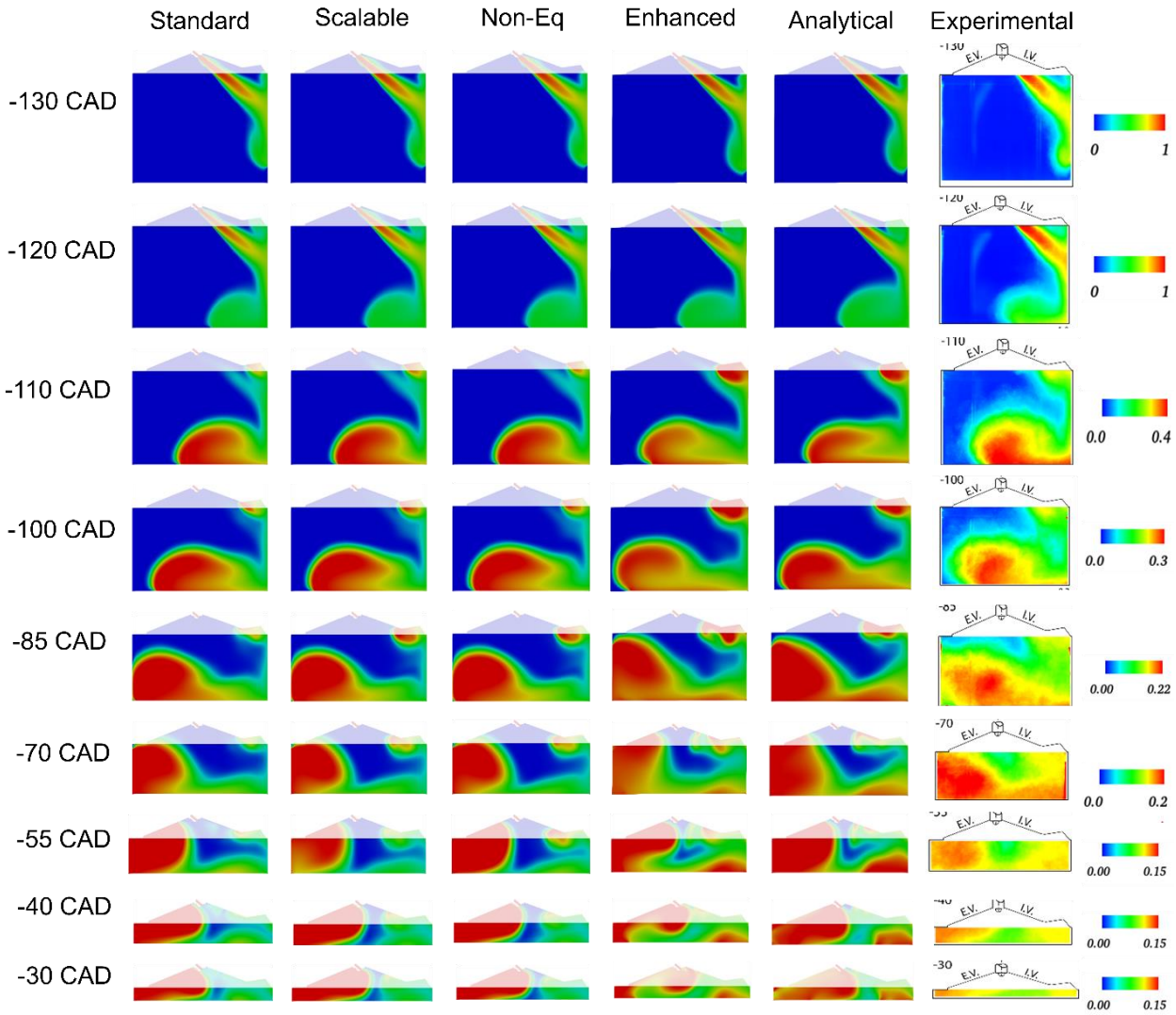

Figure 8. Comparison of hydrogen mole fraction from CFD with different wall functions against PLIF optical data

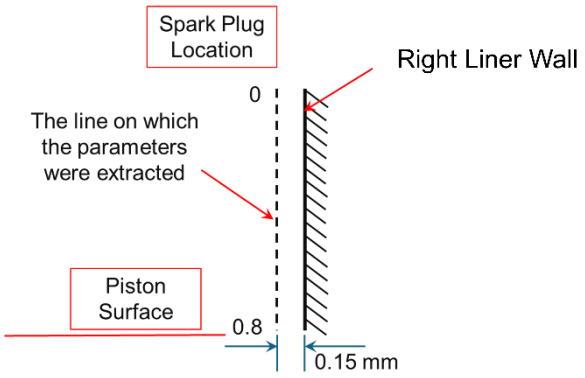

Fig. 9. A blown-up schematic of the line along which the data is extracted

An initial review of Fig. 10 reveals that the velocity profiles for the Enhanced and Analytical wall functions are comparable, while those for the Standard, Scalable, and Non-equilibrium wall functions also exhibit similarities. At -125 CAD, during the ongoing injection event, the velocity profile along the liner wall exhibits two distinct peaks. After the hydrogen jet impinges on the right liner wall (as shown in Fig. 8), a smaller portion of the gas with lower momentum (and consequently lower velocity) is deflected counterclockwise towards the spark plug, whereas the bulk of the hydrogen gas is deflected clockwise towards the piston surface with a relatively higher velocity. The first, smaller peak that occurs around 0.2 units of normalized distance along the liner corresponds to the gas mixture deflected upwards, and the second, larger peak that is observed near 0.4 units corresponds to the gas mixture deflected downwards onto the piston. With the Enhanced and Analytical wall functions, the near-wall velocity of the gas mixture near the first and second peaks is approximately 26% higher than that of the other wall functions.

Fig. 10 (b) shows the velocity of the gas near the right liner wall at -110 CAD. Although the injection event concludes at -119.5 CAD, the hydrogen gas introduced during the final phase of injection is still moving toward the liner wall by -110 CAD, as can be observed from the streak of hydrogen gas at -110 CAD (Fig 8). It is observed from Fig. 10 (b) that the Enhanced and Analytical wall functions result in approximately 27% higher velocity near the wall in the vicinity of the spark plug. In the central part of the liner, the velocity predicted by the Standard, Scalable, and Non-equilibrium wall functions is about 23% higher than that of the Enhanced and Analytical wall functions. However, the bulk of the mixture cloud at this crank angle is already on the top of the piston surface, and therefore, its momentum is not significantly affected by the near-wall velocity at the middle portion of the liner. A similar trend is observed in the near-wall velocity profile on the left liner at -100 CAD as shown in Fig. 10 (c), however, at a lower magnitude.

Fig. 11 shows the variation of the mole fraction of hydrogen in the first computational cell near the right liner wall at -125 CAD, -110 CAD, and -100 CAD for different wall functions. The x-axis in Fig. 11 remains the same as that in Fig. 10. The y-axis in Fig. 11 shows the hydrogen mole fraction with an appropriate range.

At all the considered crank angles, as shown in Fig. 11, the Enhanced and Analytical wall functions produce a richer mixture near the wall compared to the other three wall functions. At -125 CAD (Fig. 11 (a)), the Enhanced and Analytical wall functions show around 24% richer mixture near the spark plug location and around 8.5% richer mixture near the piston surface compared to the other three wall functions. At -110 CAD and -100 CAD, the near-wall hydrogen mole fraction variation follows a similar trend, though the mixture is slightly leaner at -100 CAD. As shown in Fig. 11 (b), at -110 CAD, the Enhanced and Analytical wall functions produce approximately 42% richer mixture near the spark plug compared to that produced by the other three wall functions. This can also be observed from a pocket of the rich mixture on the top right corner of the images at -110 CAD for Enhanced and Analytical wall functions as shown in Fig. 8. At the piston surface, the Enhanced and Analytical wall functions show approximately 23% richer mixture than the other

wall functions. Similarly, at -100 CAD, the mixture near the spark plug and the piston surface for the Enhanced and Analytical wall functions is richer by approximately 62% and 23%, respectively, compared to the other three wall functions.

A richer mixture combined with a higher velocity near the wall for the Enhanced and Analytical wall functions helps in a wider spread of the hydrogen mixture cloud in the combustion chamber which was discussed in Section 5.1.

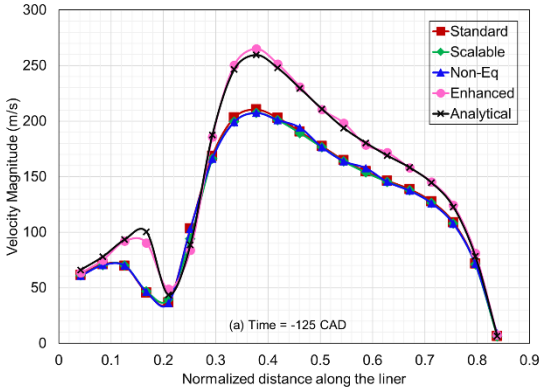

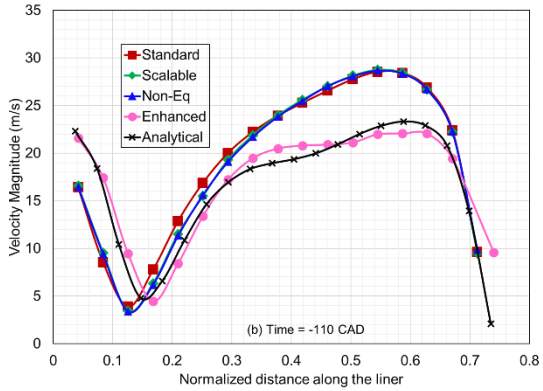

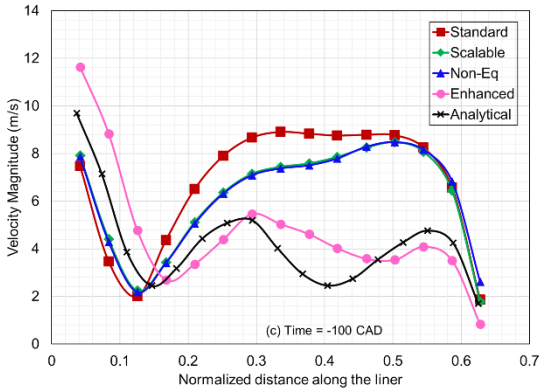

Fig. 10. Variation of the gas velocity along the right liner wall

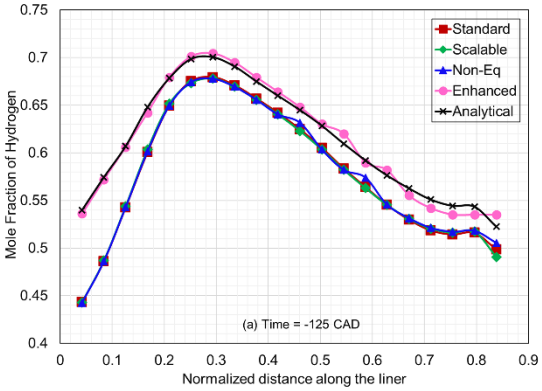

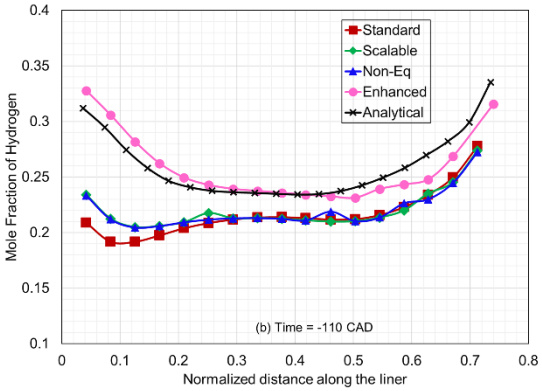

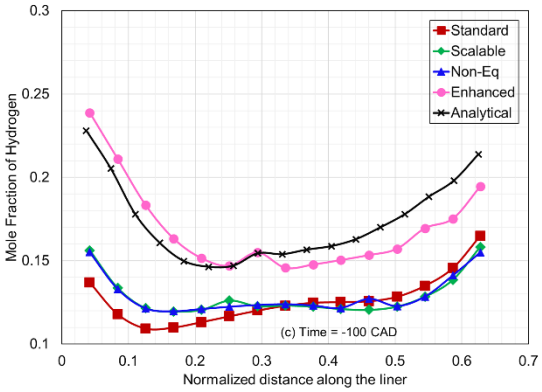

Fig. 11. Variation of the hydrogen mole fraction along the right liner wall

5.3. Impact of Wall Functions on Turbulent Kinetic Energy and Turbulent Dissipation Rate

Fig. 12 shows the variation of TKE along the right liner wall at -125 CAD, -110 CAD, and -100 CAD. Similar to the previous observations, the variation of TKE profiles for the Enhanced and Analytical wall functions are comparable while those for the Standard, Scalable, and Non-equilibrium wall functions also exhibit similarities. At -125 CAD (Fig. 12 (a)), the peak TKE for all the wall functions occurs approximately 0.3 units along the normalized distance on the liner, corresponding to the point where the high-pressure hydrogen jet impacts the liner. However, the peak TKE for the Enhanced and Analytical wall functions is approximately double as compared to the other three models. At -110 and -100 CAD (Fig. 12 (b) and (c) respectively), the TKE is higher for the Enhanced and Analytical wall functions on the liner wall in the vicinity of the spark plug region compared to the other three models. However, all the five wall functions predict similar TKE values as one moves down along the liner. As discussed earlier, the bulk of the mixture cloud has already moved away from the liner and hence its effect on the mixture distribution is negligible.

Fig. 13 shows the variation of turbulent dissipation rate along the right liner wall at -125 CAD, -110 CAD, and -100 CAD. Similar patterns can be observed in the variation of the turbulent dissipation rate, as seen with the TKE variation (Fig. 12). Higher turbulent dissipation rates at around 0.3 units of the normalized distance along the liner are observed for the Enhanced and Analytical wall functions at -125 CAD (Fig. 13 (a)) compared to the other three models. At -110 CAD and -100 CAD (Fig. 13 (b) and (c) respectively), except for the area near the spark plug on the right liner wall, the turbulent dissipation rate is generally consistent across all five wall functions. Higher turbulent dissipation rates for the enhanced and Analytical wall functions are likely the reason for better dispersion of the mixture for these cases compared to the other three wall functions.

In conclusion, the variation in TKE and turbulent dissipation rates near the right liner wall is similar between the Enhanced and Analytical wall functions, and likewise, the other three wall functions show similar behavior to each other. The Enhanced and Analytical wall functions lead to higher velocity, greater hydrogen mole fraction, increased TKE, and higher turbulent dissipation rates near the liner wall. These factors likely contribute to more effective convection and diffusion of the mixture cloud in the combustion chamber compared to the other three wall functions, thus substantiating our observations in Section 5.1.

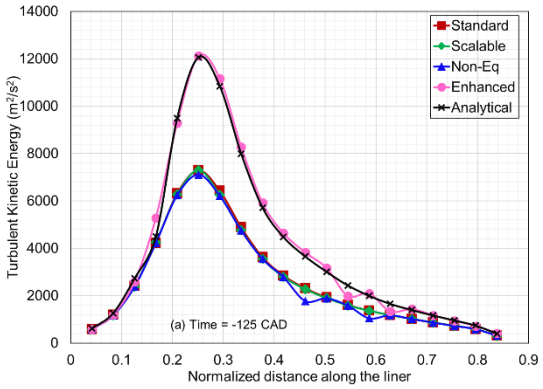

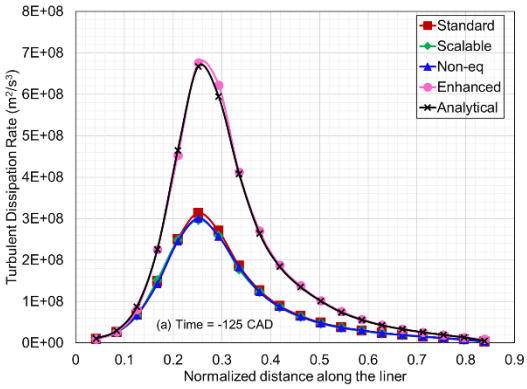

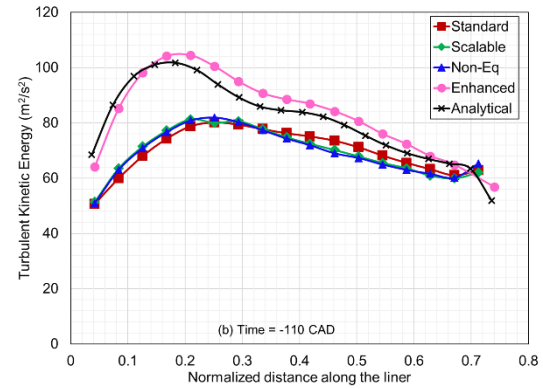

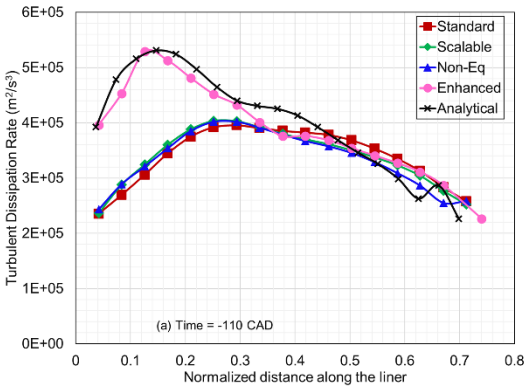

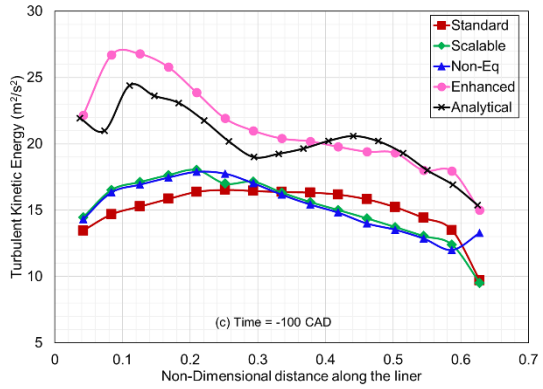

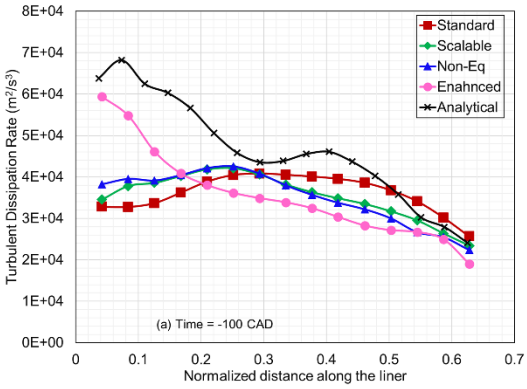

Fig. 12. Variation of the TKE along the right liner wall

Fig. 13. Variation of the Turbulence dissipation rate along the right liner wall

5.4. Comparison of the Computational Effort for Different Wall Functions

All the simulations in this study were carried out on a workstation that uses a 13th generation Intel® core™ i9 processor with 128 GB RAM and 12 CPUs. Each simulation was carried out from the IVC to the combustion TDC. Fig. 12 shows the comparison of wall time for the simulations using different wall functions. The simulation with the Non-equilibrium wall function requires the least computational time, while the one with the Enhanced wall function takes the most. The simulation

with the Enhanced wall function requires 25% more wall time compared to the Standard wall function, while the Analytical wall function simulation takes approximately 15% more wall time than the Standard wall function. It is worth noting that these simulations may take lesser computational wall time if they were to be carried out in a system with more CPUs.

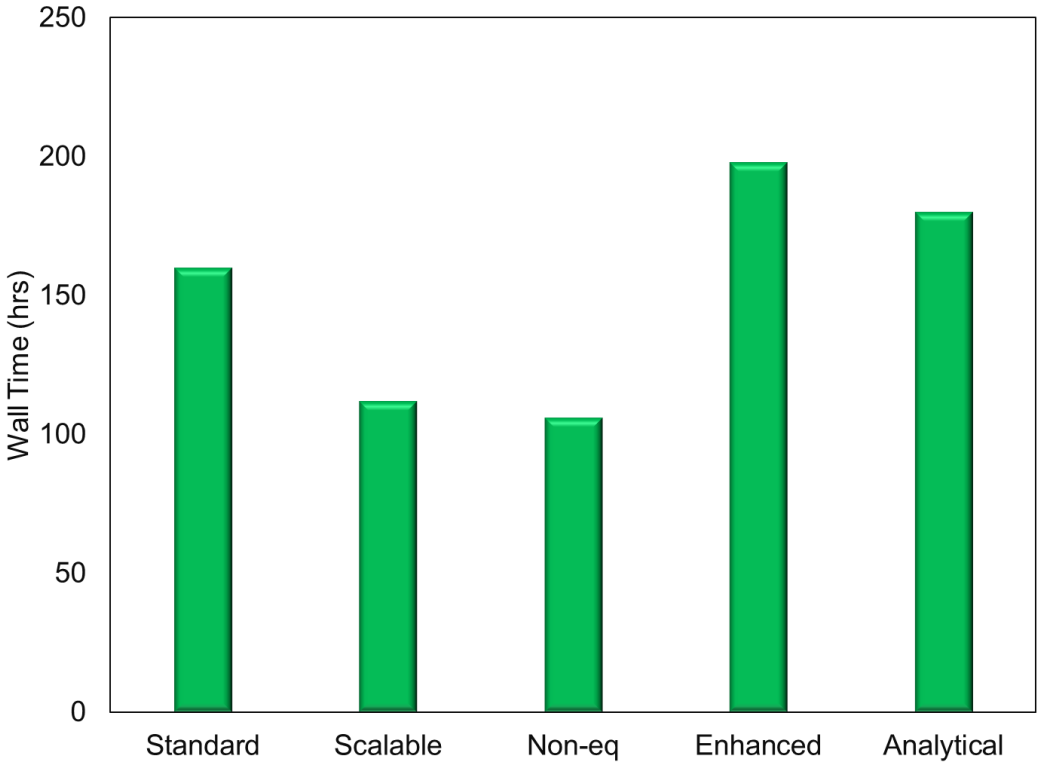

Fig. 12. Comparison of computational wall time for different wall functions

6. Conclusions

This paper investigates the effects of different wall functions commonly used to model turbulent flows near the wall on the mixture distribution in a single-cylinder direct injection spark ignition engine fueled by gaseous hydrogen. Simulations were carried out at a high tumble configuration of the engine and an injection pressure of 100 bar. Five popular wall functions, viz., standard, scalable, non-equilibrium, enhanced, and analytical, were used. The simulation results, depicting the mixture distribution in the combustion chamber at various crank angles, are compared with the experimental PLIF results reported in the literature. The following conclusions can be drawn from this study:

1. The Enhanced and Analytical wall functions enable the mixture to travel faster along the wall and achieve better dispersion compared to the other wall functions.
2. The mixture distribution predicted by the Enhanced and Analytical wall functions aligns more closely with the experimental PLIF results than the other models.

3. Both the Enhanced and Analytical wall functions predict higher velocity, increased TKE, greater mole fraction, and elevated turbulent dissipation rates compared to the other wall functions.
4. The results from the Enhanced and Analytical wall functions are consistent with each other, while the other three models exhibit similar performance.
5. The Enhanced and Analytical wall functions consume approximately 20-25% higher computation wall time compared to the Standard wall function.

In summary, the Enhanced and Analytical wall functions provide superior predictions of mixture distribution, aligning more closely with experimental PLIF results compared to other models.

CRediT authorship contribution statement

Srinivasa Krishna Addepalli: Conceptualization, Writing – review & editing, Supervision, Writing – original draft, Funding acquisition. **Arunkumar V:** Data curation, Investigation, Running the simulations, post-processing of results. **Sneha M S:** Literature review, Running the simulations, Data Curation, Writing – original draft.

Declaration of competing interest

The authors declare that they have no known competing financial interests or personal relationships that could have appeared to influence the work reported in this paper.

Acknowledgments

This work was sponsored by the Anusandhan National Research Fund – Science and Engineering Research Board (ANRF-SERB) India under the Ramanujan Fellowship (RJF/2021/000099). The authors gratefully acknowledge the computing resources provided on Lotus, a high-performance computing cluster at the Indian Institute of Technology Tirupati (IITT). The authors acknowledge the data provided on the Sandia website, which helped in validating the CFD model. The authors would also like to acknowledge Convergent Science Inc. for providing licenses for the CONVERGE software.

7. References

1. Onorati, A., Payri, R., Vaglieco, B., Agarwal, A., Bae, C., Bruneaux, G., Canakci, M., Gavaises, M., Günthner, M., Hasse, C., Kokjohn, S., Kong, C., Moriyoshi, Y., Novella, R., Pesyridis, A., Reitz, R., Ryan, T., Wagner, R., & Zhao, H. (2022). The role of hydrogen for future internal combustion engines. International Journal of Engine Research. 23 (4), https://doi.org/10.1177/14680874221081947.
2. Le, T. S., Nguyen, T. N., Bui, D., & Ngo, T. D. (2023). Optimal sizing of renewable energy storage: A techno-economic analysis of hydrogen, battery, and hybrid systems considering degradation and seasonal storage. Applied Energy, 336, 120817. https://doi.org/10.1016/j.apenergy.2023.120817.

3. Marocco, P., Novo, R., Lanzini, A., Mattiazzo, G., & Santarelli, M. (2022). Towards 100% renewable energy systems: The role of hydrogen and batteries. Journal of Energy Storage, 57, 106306. https://doi.org/10.1016/j.est.2022.106306.
4. Bhogilla, S., Pandoh, A., & Singh, U. R. (2024). Cogeneration system combining reversible PEM fuel cell, and metal hydride hydrogen storage enabling renewable energy storage: Thermodynamic performance assessment. International Journal of Hydrogen Energy, 52, 1147-1155. https://doi.org/10.1016/j.ijhydene.2023.08.028.
5. Mayyas, A., Wei, M., & Levis, G. (2020). Hydrogen as a long-term, large-scale energy storage solution when coupled with renewable energy sources or grids with dynamic electricity pricing schemes. International Journal of Hydrogen Energy, 45(33), 16311-16325. https://doi.org/10.1016/j.ijhydene.2020.04.163.
6. Arsad, A., Hannan, M., Al-Shetwi, A. Q., Mansur, M., Muttaqi, K., Dong, Z., & Blaabjerg, F. (2022). Hydrogen energy storage integrated hybrid renewable energy systems: A review analysis for future research directions. International Journal of Hydrogen Energy, 47(39), 17285-17312. https://doi.org/10.1016/j.ijhydene.2022.03.208.
7. Ferraren-De Cagalitan, D., & Abundo, M. (2021). A review of biohydrogen production technology for application towards hydrogen fuel cells. Renewable and Sustainable Energy Reviews, 151, 111413. https://doi.org/10.1016/j.rser.2021.111413.
8. Pramuanjaroenkij, A., & Kakaç, S. (2023). The fuel cell electric vehicles: The highlight review. International Journal of Hydrogen Energy, 48(25), 9401-9425. https://doi.org/10.1016/j.ijhydene.2022.11.103.
9. Singla, M.K., Nijhawan, P. & Oberoi, A.S. Hydrogen fuel and fuel cell technology for cleaner future: a review. Environ Sci Pollut Res 28, 15607–15626 (2021). https://doi.org/10.1007/s11356-020-12231-8.
10. Ajanovic, A., & Haas, R. (2021). Prospects and impediments for hydrogen and fuel cell vehicles in the transport sector. International Journal of Hydrogen Energy, 46(16), 10049-10058. https://doi.org/10.1016/j.ijhydene.2020.03.122.
11. Miller EL, Thompson ST, Randolph K, Hulvey Z, Rustagi N, Satyapal S. US Department of Energy hydrogen and fuel cell technologies perspectives. MRS Bulletin. 2020;45(1):57-64. https://doi.org/10.1557/mrs.2019.312.
12. Boretti, A. (2020). Hydrogen internal combustion engines to 2030. International Journal of Hydrogen Energy, 45(43), 23692-23703. https://doi.org/10.1016/j.ijhydene.2020.06.022.
13. Falfari, S., Cazzoli, G., Mariani, V., & Bianchi, G. M. (2022). Hydrogen Application as a Fuel in Internal Combustion Engines. Energies, 16(6), 2545. https://doi.org/10.3390/en16062545.
14. Teoh, Y. H., How, H. G., Le, T. D., Nguyen, H. T., Loo, D. L., Rashid, T., & Sher, F. (2023). A review on production and implementation of hydrogen as a green fuel in internal combustion engines. Fuel, 333, 126525. https://doi.org/10.1016/j.fuel.2022.126525.
15. Zhu, H., Zhang, Y., Liu, F., & Wei, W. (2020). Effect of excess hydrogen on hydrogen fueled internal combustion engine under full load. International Journal of Hydrogen Energy, 45(39), 20419-20425. https://doi.org/10.1016/j.ijhydene.2019.12.022.

16. Boretti, A. (2024). Phased transition from methane to hydrogen in internal combustion engines: Utilizing hythane and direct injection jet ignition for enhanced efficiency and reduced emissions. International Journal of Hydrogen Energy, 80, 1255-1265. https://doi.org/10.1016/j.ijhydene.2024.07.251.
17. Akal, D., Öztuna, S., & Büyükakın, M. K. (2020). A review of hydrogen usage in internal combustion engines (gasoline-Lpg-diesel) from combustion performance aspect. International Journal of Hydrogen Energy, 45(60), 35257-35268. https://doi.org/10.1016/j.ijhydene.2020.02.001.
18. Yip HL, Srna A, Yuen ACY, Kook S, Taylor RA, Yeoh GH, Medwell PR, Chan QN. A Review of hydrogen direct injection for internal combustion engines: towards carbon-free combustion. Appl Sci 2019;9(22). https://doi.org/10.3390/app9224842.
19. Koyanagi K, Hiruma M, Furuhama S. Study on mechanism of backfire in hydrogen engines. SAE Technical Paper 942035. 1994. https://doi.org/10.4271/942035.
20. Kondo T, Iio S, Hiruma M. A Study on the mechanism of backfire in external mixture formation hydrogen engines - about backfire occurred by cause of the spark plug. SAE Technical Paper 971704. 1997. https://doi.org/10.4271/971704.
21. Guo LS, Lu HB, Li JD. A hydrogen injection system with solenoid valves for a four-cylinder hydrogen-fueled engine. Int J Hydrogen Energy 1999;24(4):377e82. https://doi.org/ 10.1016/S0360-3199(98)00035-4.
22. Zeyuan Huang, Shuang Yuan, Hong Wei, Lijia Zhong, Zhen Hu, Zongkuan Liu, Changwen Liu, Haiqiao Wei, Lei Zhou, Effects of hydrogen injection timing and injection pressure on mixture formation and combustion characteristics of a hydrogen direct injection engine, Fuel, Volume 363, 2024, 130966, ISSN 0016-2361, https://doi.org/10.1016/j.fuel.2024.130966.
23. Zhen Hu, Shuang Yuan, Hong Wei, Zeyuan Huang, Haiqiao Wei, Siew Hwa Chan, Lei Zhou, High-pressure injection or low-pressure injection for a direct injection hydrogen engine, International Journal of Hydrogen Energy, Volume 59, 2024, Pages 383-389, ISSN 0360-3199, https://doi.org/10.1016/j.ijhydene.2024.02.018.
24. A. Scalambro, A. Piano, F. Millo, N. Scinicariello, W. Lodi, A. Dhongde, G. Sammito, Numerical analysis of the hydrogen-air mixture formation process in a direct-injection engine for off-road applications, International Journal of Hydrogen Energy, Volume 77, 2024, Pages 1286-1295, ISSN 0360-3199, https://doi.org/10.1016/j.ijhydene.2024.06.193.
25. Yinmi Luo, Binyang Wu, Qian Li, Xuelin Tang, Zhiyong Yang, Chunling Wu, Taoyang Wu, Experimental and simulation research on the lean combustion characteristics of direct-injection hydrogen engine, International Journal of Hydrogen Energy, Volume 68, 2024, Pages 398-409, ISSN 0360-3199, https://doi.org/10.1016/j.ijhydene.2024.04.184.
26. Bifen Wu, Roberto Torelli, Yuanjiang Pei, Numerical modeling of hydrogen mixing in a direct-injection engine fueled with gaseous hydrogen, Fuel, Volume 341, 2023, 127725, ISSN 0016-2361, https://doi.org/10.1016/j.fuel.2023.127725.

27. Wang, Y., Evans, A., Srna, A., Wehrfritz, A. et al., "A Numerical Investigation of Mixture Formation and Combustion Characteristics of a Hydrogen-Diesel Dual Direct Injection Engine," SAE Technical Paper 2021-01-0526, 2021, https://doi.org/10.4271/2021-01-0526.
28. Salazar, V. and Kaiser, S., "Influence of the In-Cylinder Flow Field (Tumble) on the Fuel Distribution in a DI Hydrogen Engine Using a Single-Hole Injector," SAE Int. J. Engines 3(1):309-325, 2010, https://doi.org/10.4271/2010-01-0579.
29. Scarcelli, R., Wallner, T., Salazar, V., and Kaiser, S., "Modeling and Experiments on Mixture Formation in a Hydrogen Direct-Injection Research Engine," SAE Int. J. Engines 2(2):530-541, 2010, https://doi.org/10.4271/2009-24-0083.
30. Sujith Sukumaran, Song-Charng Kong, Numerical study on mixture formation characteristics in a direct-injection hydrogen engine, International Journal of Hydrogen Energy, Volume 35, Issue 15, 2010, Pages 7991-8007, ISSN 0360-3199, https://doi.org/10.1016/j.ijhydene.2010.05.090.
31. Xiumin Yu, Guanting Li, Wei Dong, Zhen Shang, Zezhou Guo, Yinan Li, Decheng Li, Zhe Zhao, Numerical study on effects of hydrogen direct injection on hydrogen mixture distribution, combustion and emissions of a gasoline/hydrogen SI engine under lean burn condition, International Journal of Hydrogen Energy, Volume 45, Issue 3,2020,Pages 2341-2350,ISSN 0360-3199, https://doi.org/10.1016/j.ijhydene.2019.11.048.
32. Zhen Fu, Wenzhi Gao, Yuhuai Li, Xinyu Hua, Jiahua Zou, Yong Li, Numerical simulation of the mixture distribution and its influence on the performance of a hydrogen direct injection engine under an ultra-lean mixture condition, International Journal of Hydrogen Energy, Volume 48, Issue 51, 2023, Pages 19700-19712, ISSN 0360-3199, https://doi.org/10.1016/j.ijhydene.2023.02.041.
33. H. Che and V. Patel, "Practical near-wall turbulence models for complex flows including separation," AIAA 1987-1300. 19th AIAA, Fluid Dynamics, Plasma Dynamics, and Lasers Conference. June 1987, https://doi.org/10.2514/6.1987-1300.
34. Fadhila, H., Medina, H., Aleksandrova, S., & Benjamin, S. (2020). A new non-linear RANS model with enhanced near-wall treatment of turbulence anisotropy. Applied Mathematical Modelling, 82, 293-313. https://doi.org/10.1016/j.apm.2020.01.056
35. Berni, F., & Fontanesi, S. (2020). A 3D-CFD methodology to investigate boundary layers and assess the applicability of wall functions in actual industrial problems: A focus on in-cylinder simulations. Applied Thermal Engineering, 174, 115320. https://doi.org/10.1016/j.applthermaleng.2020.115320
36. Salazar VM, Kaiser SA. An optical study of mixture preparation in a hydrogen-fueled engine with direct injection using different nozzle designs. SAE Int J Eng 2010;2(2). https://doi.org/10.4271/2009-01-2682.
37. Salazar VM, Kaiser SA. Characterization of mixture reparation in a direct-injection internal combustion engine fueled with hydrogen using PIV and PLIF. In: 15th International symposium on applications of laser techniques to fluid mechanics, Lisbon, July 5-8; 2010.
38. https://ecn.sandia.gov/engines/hydrogen-engine.

39. Le Moine J, Kaiser SA, Salazar VM, Anders JW, Svensson KI, Gehrke C,R. A computational study of the mixture preparation in a directeinjection hydrogen engine. J Eng Gas Turbines Power 2015;137. https://doi.org/10.1115/1.4030397.
40. Lucchini T, D'Errico G, Fiocco M. Multi-dimensional modeling of gas exchange and fuel-air mixing processes in a direct injection, gas-fueled engine. SAE Technical Paper 2011-24-0036. 2011. https://doi.org/10.4271/2011-24-0036
41. Federico Ramognino, Lorenzo Sforza, Gianluca D'Errico, Josep Gomez-Soriano, Angelo Onorati, Ricardo Novella, CFD Modelling of Hydrogen-Fueled SI Engines for Light-Duty Applications. SAE Technical paper, 2023-24-0017, 2023. https://doi.org/10.4271/2023-24-0017
42. Addepalli, S. K., Pei, Y., Zhang, Y., & Scarcelli, R. (2022). Multi-dimensional modeling of mixture preparation in a direct injection engine fueled with gaseous hydrogen. International Journal of Hydrogen Energy, 47(67), 29085-29101. https://doi.org/10.1016/j.ijhydene.2022.06.182
43. Wu, B., Torelli, R., & Pei, Y. (2023). Numerical modeling of hydrogen mixing in a direct-injection engine fueled with gaseous hydrogen. Fuel, 341, 127725. https://doi.org/10.1016/j.fuel.2023.127725
44. Scarcelli, R., Wallner, T., Matthias, N., Salazar, V. et al., "Numerical and Optical Evolution of Gaseous Jets in Direct Injection Hydrogen Engines," SAE Technical Paper 2011-01-0675, 2011, https://doi.org/10.4271/2011-01-0675.
45. Scarcelli R, Wallner T, Matthias N, Salazar V, Kaiser SA. Mixture formation in direct injection hydrogen engines: CFD and optical analysis of single- and multi-hole nozzles. SAE Int J Eng 2011;4(2):2361-75. https://doi.org/10.4271/2011-24-0096.
46. Nasrifar K. Comparative study of eleven equations of state in predicting the thermodynamic properties of hydrogen. Int J Hydrogen Energy 2010;35(8):3802-11. https://doi.org/10.1016/j.ijhydene.2010.01.032.
47. Kim, S.-E., and Choudhury, D., "A Near-Wall Treatment Using Wall Functions Sensitized to Pressure Gradient," Separated and Complex Flows, 217, 273-280, 1995.
48. White, F.M. and Christoph, G.H., "A Simple Theory for the Two-Dimensional Compressible Turbulent Boundary Layer," Journal of Basic Engineering, 94(3), 636-642, 1972. https://doi.org/10.1115/1.3425519

Declaration of interests

☒ The authors declare that they have no known competing financial interests or personal relationships that could have appeared to influence the work reported in this paper.

☐The authors declare the following financial interests/personal relationships which may be considered as potential competing interests:

The authors declare that they have no known competing financial interests or personal relationships that could have appeared to influence the work reported in this paper.